Journal of Photochemistry and Photobiology A: Chemistry 212 (2010) 170–175

Contents lists available at ScienceDirect

Journal of Photochemistry and Photobiology A: Chemistry

journal homepage: www.elsevier.com/locate/jphotochem

Synthesis, characterization and optical properties of organic nanoparticles of piroxicam anti-inflammatory drug

Maged El-Kemary[b], Hiroshi Yao[a,*]

[a] Graduate School of Material Science, University of Hyogo, 3-2-1 Koto, Kamigori-cho, Ako-gun, Hyogo 678-1297, Japan
[b] Department of Chemistry, Faculty of Science, Kafr ElSheikh University, 33516 Kafr ElSheikh, Egypt

ARTICLE INFO

Article history:
Received 2 October 2009
Received in revised form 30 March 2010
Accepted 19 April 2010
Available online 27 April 2010

Keywords:
Piroxicam organic nanoparticles
Ion association
Optical properties
Emission enhancement
Drug

ABSTRACT

We report the synthesis, characterization and optical properties of "anionic" drug-based organic nanoparticles. Aqueous-phase ion association between piroxicam (PX) anion and lipophilic phosphazenium cation such as tetrakis[tris(dimethylamino)phosphoranylideneamino]phosphonium (PHS), in the presence of polyvinylpyrrolidone (PVP), produces PX nanoparticles of 200–400 nm in diameter. The stability of the nanoparticles is dependent on the molar ratio (ρ) of the loaded cation to the drug anion, giving an appropriate synthetic condition of $\rho = 1.5$. The PX nanoparticles exhibit an enhanced emission with a bathochromic shift compared to that of the PX monomer in water, but their absorption properties do not change. The emission enhancement is due to the effect of immobilization of PX in the hydrophobic solid-state matrices.

1. Introduction

Currently, nanomaterials have been applied in medical diagnosis and drug delivery technology [1–7], which can bring both commercial and therapeutic values to health care products [6]. The selective delivery of drugs to their site of action should increase therapeutic effectiveness and reduce harmful systematic effects. Optimising the experimental conditions for design of organic drug nanoparticles and a detailed understanding of their optical and chemical properties are essential in drug delivery. As already reported, the optical properties of drug inside nanoparticles significantly differ from those of monomeric species [8].

Meanwhile, we have reported the synthesis of organic nanoparticles with controllable size and their interesting optical properties in pure aqueous media [8–12]. The preparation method is based on the hydrophobic ion-pair formation between functional organic ions and hydrophobic counterions to fabricate nano-architectures in water (ion-association technique). In organic nanoparticles, weak van der Waals intermolecular and hydrogen-bonding interactions are responsible for the specific electronic/optical properties that are fundamentally different from those of inorganic metals or semiconductors [13]. Therefore, fabrication of organic nanoparticles have recently seen an increasing level of academic or industrial research [14–16] due to a much larger commercial opportunity in the thousands of organic compounds that are used across many high-technology and commodity product areas. In particular, nanoformulations of many developed organic drugs have raised promising potential for improving drug bioavailability. Inclusion of drug molecules into cyclodextrin cavity is usually used for this purpose, but a major disadvantage lies in the limiting number of drugs exhibiting good fit into the cyclodextrin cavity. The production of drug nanoparticles has been then developed as one of the ideal approaches to overcome such problems [17].

Piroxicam (PX), shown in Fig. 1, is a non-steroidal anti-inflammatory organic drug with unwanted side effect during the therapy [18]. At neutral pH, it adopts an anionic structure [19]. The binding properties and the dynamics of the interaction of PX caged to human serum albumin protein, cyclodextrins, and micelles were studied [20–23], elucidating that the spectral changes reflect the hydrophobic interaction of the cage with drug [20]. In addition, the photophysics and photochemistry of PX in solution have been the subject of many experimental steady-state and time-resolved studies [21,24,25]. Some of the most important early findings are as follows: (a) PX exhibits an internal twisting motion to generate the keto rotamers in 2–5 ps [24]; (b) the enol form of PX undergoes excited state intramolecular proton-transfer reaction with time <100 fs to produce a keto form [25]; (c) the fluorescence quantum yield of piroxicam in water is very low (0.01×10^{-2}) [25] and (d) it forms intermolecular hydrogen bonds with water [25]. These findings indicate the existence of a rapid nonradiative decay processes from the excited state. Very

* Corresponding author. Fax: +81 791 58 0161.
E-mail addresses: elkemary@yahoo.com (M. El-Kemary), yao@sci.u-hyogo.ac.jp (H. Yao).

1010-6030/$ – see front matter © 2010 Elsevier B.V. All rights reserved.
doi:10.1016/j.jphotochem.2010.04.012

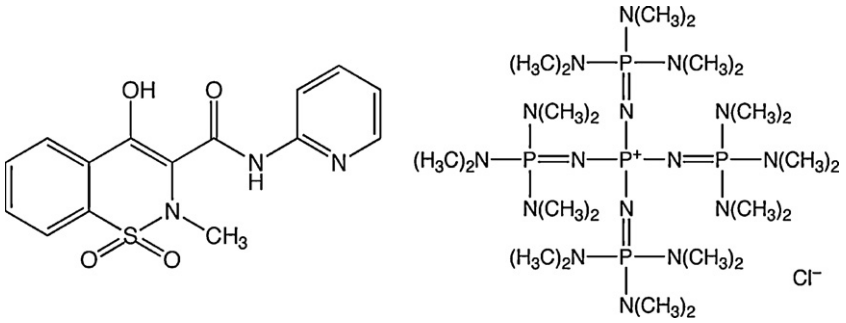

Fig. 1. Structures of piroxicam (abbreviated as PX; left) and PHS chloride (right).

recently, piroxicam:Eudragit®RS100 nanoparticles was formulated using a complicated solvent-evaporation/extraction technique [3]. The nanoparticles were then used to assess the anti-inflammatory impacts of piroxicam nanoparticles in the rabbits with endotoxin-induced uveitis [3].

The aim of this work is to prepare and characterize "anionic" PX-based organic nanoparticles using the ion-association technique. The production of organic nanoparticles using functional "cationic" molecules has been successful; however, the simple and versatile synthesis of anion-based organic nanoparticles remains a major challenge. We find that ion association between PX anion and lipophilic phosphazenium cation (tetrakis[tris(dimethylamino)-phosphoranylideneamino]phosphonium (PHS) cation), in the presence of polyvinylpyrrolidone (PVP), produces the drug nanoparticles of 200–400 nm in aqueous solution. The ion-association technique does not require longer processing times to achieve nano-sized organic particles.

2. Experimental

2.1. Materials

Piroxicam (1,2-benzothiazine-3-carboxamide-4-hydroxy-2-methyl-*N*-(2-pyridyl)-1,1-dioxide, abbreviated as PX; Fig. 1) was purchased from Sigma and used as received. Polyvinylpyrrolidone (abbreviated as PVP; average MW = 10,000, Aldrich) was used as a neutral stabilizer to prevent particle agglomeration, and tetrakis[tris(dimethylamino)phosphoranylideneamino]phosphonium chloride (abbreviated as PHS, Fluka, Fig. 1) were of the highest commercial grade available and used without further purification. PHS is one of the delocalized hydrophobic bulky cations that are occasionally used for ion-pair extractions [26]. Pure water was obtained by an Advantec GS-200 automatic water distillation supplier. Basic solution of pH 11 was prepared by adding an appropriate amount of 0.1 M sodium hydroxide solution from Wako.

2.2. Synthesis of PX nanoparticles

PX nanoparticles were prepared by means of the ion-association technique [9]. The PX possesses a very low solubility in water of pH 7 and its solubility increase significantly with increasing the pH value. Therefore we used aqueous solution of pH 11 for preparing the nanoparticles. Under this condition, PX is fully deprotonated to form anionic species (in the form of $-O^-$ of the benzothiazine ring). A typical preparation procedure is depicted as follows: at room temperature, the addition of an equal volume of aqueous PX solution (0.1 mM) to an aqueous solution containing PHS (0.1–0.15 mM) and PVP under ultrasonication produced a suspension of nanoparticles. Namely ion association between the PX anions and PHS cations leads to nanoparticle formation. Further sonication was continued for 10 min. The concentrations of the starting compounds (PX, PHS and PVP) were optimised by modelling the molar ratio (ρ) of PHS to PX (that is, $\rho = [PHS^+]/[PX^-]$), and by changing the concentration of PVP to obtain small nanoparticles with reproducible properties and with relatively high fluorescence efficiency compared to that of the PX monomer in water. The final PVP concentration ranged from 0.2 to 0.4 mg/mL. Herein we call such particles "PX nanoparticles" because their optical properties are dominated by the PX chromophore. For concise, PX nanoparticles prepared using PX (0.1 mM) and PHS (0.15 mM) are referred to as PX23a, PX23b, and PX23c for [PVP] of 0.2, 0.3, and 0.4 mg/mL, respectively, whereas that prepared using PX (0.1 mM), PHS (0.1 mM), and PVP (0.2 mg/mL) is referred to as PX11a. It should be noted that the final drug concentration was a half of the initial concentration, that is, 0.05 mM. Moreover, the final molar ratio of PHS cations to PX anions, determined as ρ, was 1.5 or 1.0.

Mixing of aqueous PHS and PX solutions at the same fraction in the absence of PVP yielded pale greenish yellow opaque solid dispersion composed of the anion-exchanged drug species, PX–PHS, which precipitated with time. We isolated these precipitates by removal of the aqueous layer followed by three repeated washing with water and drying under vacuum. The PX–PHS solids were insoluble in water but soluble in chloroform, so their spectroscopic properties were evaluated in chloroform.

2.3. Instrumentation

The morphology and size of PX nanoparticles were examined with a Hitachi S-4800 scanning transmission electron microscope (STEM). A specimen for STEM observations was prepared by dropping the suspension on an amorphous carbon-coated copper mesh. The measurements of the hydrodynamic diameter of nanoparticles on the basis of dynamic light scattering (DLS) in aqueous solution were conducted with an Otsuka ELS-800 light scattering spectrophotometer with a 10-mW He–Ne laser. The X-ray diffraction (XRD) measurements were conducted by using Rigaku RINT-2000 with Cu Kα tube attaching a graphite monochromator. FT-IR spectra were measured with a Horiba FT-720 infrared spectrophotometer. UV–visible absorption spectra were recorded on a Hitachi U-4100 spectrophotometer. Fluorescence spectra were obtained with a Hitachi F-4500 spectrofluorometer.

3. Results and discussion

3.1. Characterization and optical properties of the PX–PHS solid in chloroform

Fig. 2A shows the absorption spectra of pure PX, PHS and PX–PHS precipitate in chloroform at room temperature. It is apparent that PHS has no significant absorption, whereas PX displays sharp absorption peek at 327 nm. However, PX–PHS exhibited a

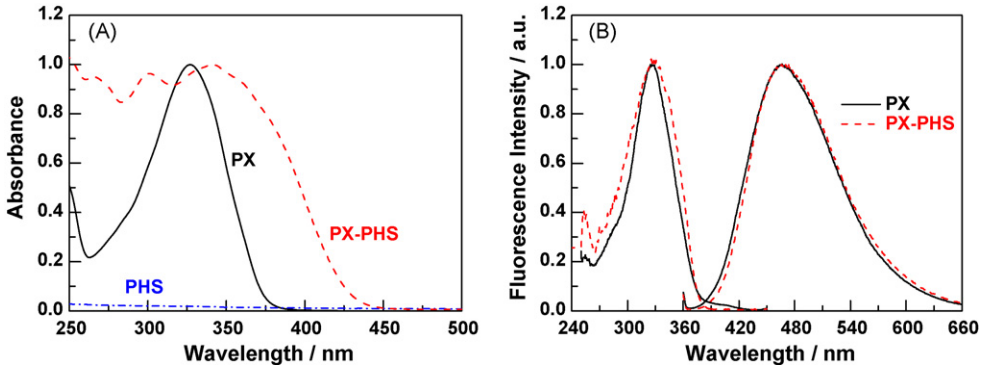

Fig. 2. (A) Absorption spectra of PX, PHS and PX–PHS in chloroform. (B) Fluorescence emission (right, λ_{ex} = 365 nm) and excitation spectra (left, λ_{em} = 465 nm) of PX and PX–PHS in chloroform.

red-shifted broad absorption peak with a maximum at 341 nm and a tail around 400–450 nm. The red-shifted absorption spectrum suggests that PX–PHS is present in the form of an ion-pair complex in less-polar chloroform solvent [12]. The change of the spectral shape implies that the absorption spectra are probably a composite of two different transitions. The tail is likely to be $n \rightarrow \pi^*$ ($S_0 \rightarrow S_1$) transition which is partially hidden by stronger $\pi \rightarrow \pi^*$ ($S_0 \rightarrow S_1$) absorption. On the other hand, the emission spectrum of PX–PHS undergoes a minor red-shift of 2 nm in comparison with that of PX (Fig. 2B). The fluorescence excitation spectrum of PX–PHS monitored at 465 nm was quite different form the absorption, but similar with that of PX with a slightly broader spectral shape. These results suggest that there may be a strong ion-pair interaction in the ground state compared to that in the excited state.

It should be noted that the emission spectrum of PX in less-polar chloroform exhibited a blue shift compared to that in water with higher polarity and hydrogen-bonding ability (Table 1). This shift is due to an intramolecular hydrogen bond between the –OH group of the benzothiazine ring and the carbonyl of the lateral amide group, forming a six-membered ring [19]. This process is perturbed in protic solvents by the formation of an intermolecular hydrogen bond producing an open conformer or even the anionic species due to a very low pK_a (~4.9) [25]. Therefore, in water solution, the observed fluorescence quantum yield (0.01×10^{-2}) is significantly lower than that in chloroform (0.19×10^{-2}), see Table 1, due to efficient nonradiative channels involving an intermolecular hydrogen bond with water molecules.

Fig. 3 shows the XRD pattern of the PX–PHS solid. Well-defined peaks observed at specific angles in the diffraction pattern indicate a crystalline nature of the sample. The inset depicts a typical STEM image of the sample. The image revealed that the precipitates have crystalline facets suggesting also the crystalline nature. The FT-IR spectrum of the PX–PHS precipitate shows approximate superimposition of the patterns of drug and PHS (Fig. 4), indicating no strong chemical interactions between PX anions and PHS cations in the solid precipitate. Therefore, there are no new

Table 1
Fluorescence peak positions and quantum yields (Φ_f) of various samples containing PX chromophore under an aerated condition.

Sample	Phase	Fluorescence/nm	Φ_f[a]/10^{-2}
PX	Aqueous	480	0.01[b]
PX	Chloroform	468	0.19[b]
PX–PHS	Chloroform	470	0.22
PX23a	Nanoparticles (d_{av} = 364 nm)	502	0.08
PX23b	Nanoparticles (d_{av} = 348 nm)	502	0.09
PX23c	Nanoparticles (d_{av} = 232 nm)	502	0.10

[a] Φ_f: ±10%.
[b] Ref. [25].

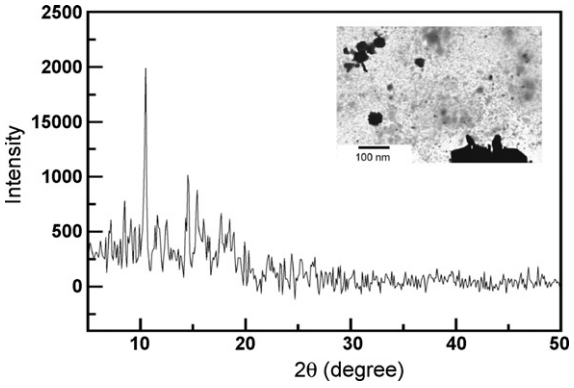

Fig. 3. XRD pattern of the PX–PHS precipitate. The inset shows a typical STEM image of the precipitate, representing crystalline facets.

supply chain issues and existing understanding of long-term environmental effects and fate can be used to evaluate new product. A similar behaviour was also observed for PX:Eudragit®RS100 [3] and flurbiporfen:Eudragit®RS100 nanosuspensions [27].

3.2. Formation of organic PX nanoparticles

We have prepared a series of PX nanoparticles in aqueous solutions of pH 11 in the presence of PVP by the ion-association method [9]. Fig. 5a shows a typical photograph of the aqueous dispersions of PX11a (ρ = 1) and PX23a (ρ = 1.5) samples. The solution prepared

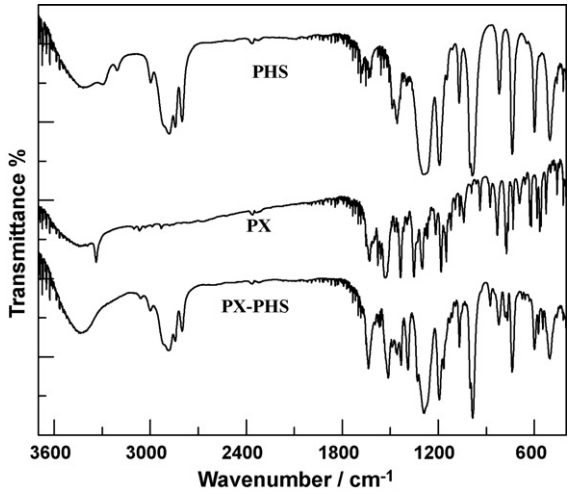

Fig. 4. FT-IR spectra of PHS chloride, PX, and their PX–PHS precipitate.

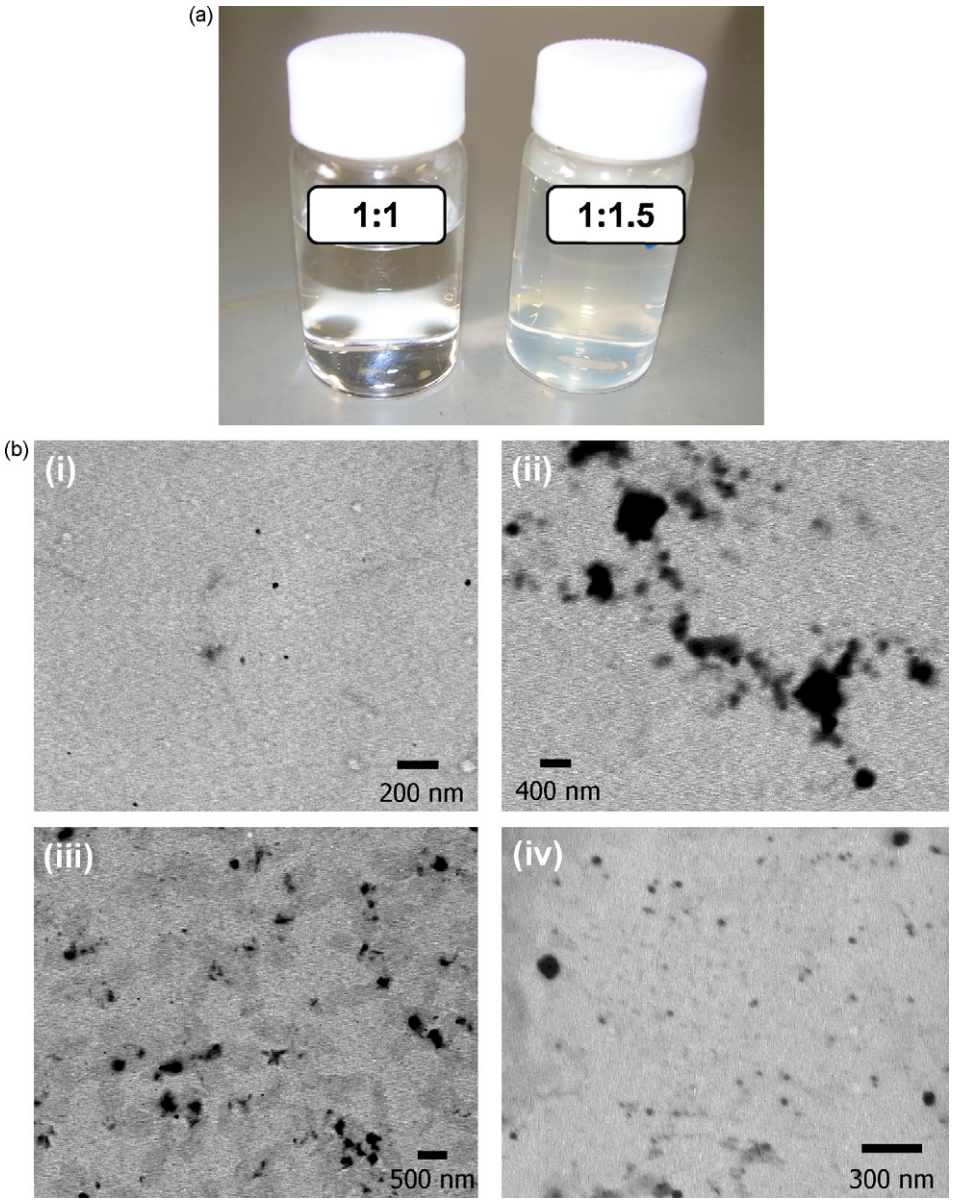

Fig. 5. (a) Photograph of PX11a (left) and PX23b (right). (b) Representative STEM images of the samples: (i) PX11a, (ii) PX23a, (iii) PX23b and (iv) PX23c.

at $\rho = 1$ was colourless and highly transparent solution, as shown in the left. On the other hand, well-dispersible particles with slight light scattering were visible in the homogeneous aqueous solution, as shown in the right.

The sample morphology and size were obtained by STEM and DLS analyses. Fig. 5b shows a typical STEM image of the sample PX11a, PX23a, PX23b or PX23c. In sample PX11a, the STEM image clarified the nearly absence of particles, as a consequence, we could not conduct the DLS measurements for this sample. This suggests that PX nanoparticles are probably unstable at the experimental condition of $\rho = 1$ in the presence of PVP, and a higher ρ value would be preferable to stabilize the nanoparticles. Fig. 5b(ii)–(iv) display the PX nanoparticles prepared at $\rho = 1.5$ with the size range of 200–600, 50–400, and 10–150 nm in diameter, respectively. The particle size decreases with an increase in the concentration of PVP from 0.2 to 0.4 mg/mL. In addition, the micrographs show that a higher concentration of PVP is effective to protect PX nanoparticles from aggregation. It should be noted that increasing the ρ value into 2 (data are not shown) induced faster aggregation of the particles at the same PVP concentration, indicating that adsorption of the excess phosphazenium cation (PHS^+) onto nanoparticles does not play a role in effectively stabilizing the nanoparticles. This is probably due to a steric effect, which competes with van der Waals and electrostatic interactions, and can promote faster aggregation.

Fig. 6a–c shows the particle size distributions of PX23a, PX23b and PX23c nanoparticles in aqueous solution determined by DLS. For PX23a and PX23b samples with relatively low PVP concentrations, bimodal size distributions are observed. The major component is due to the small (several hundreds of nanometers) nanoparticles and the minor one (inset of Fig. 6a and b) is due to the flocculates. Interestingly, the PX23c nanoparticles obtained with the highest PVP concentration (0.4 mg/mL) displayed a unimodal distribution with relatively smaller size. The average diameters of the samples PX23a, PX23b and PX23c are obtained to be 364, 348, and 232 nm, respectively, with a standard deviation of ~15%. Note that the diameters determined by DLS are slightly larger than those obtained by STEM probably due to the presence of the flocculates, but nearly in agreement with observations. The obtained average particle diameters are resultantly comparable with that reported (230–250 nm) for PX:Eudragit®RS100 nanoparticles [3].

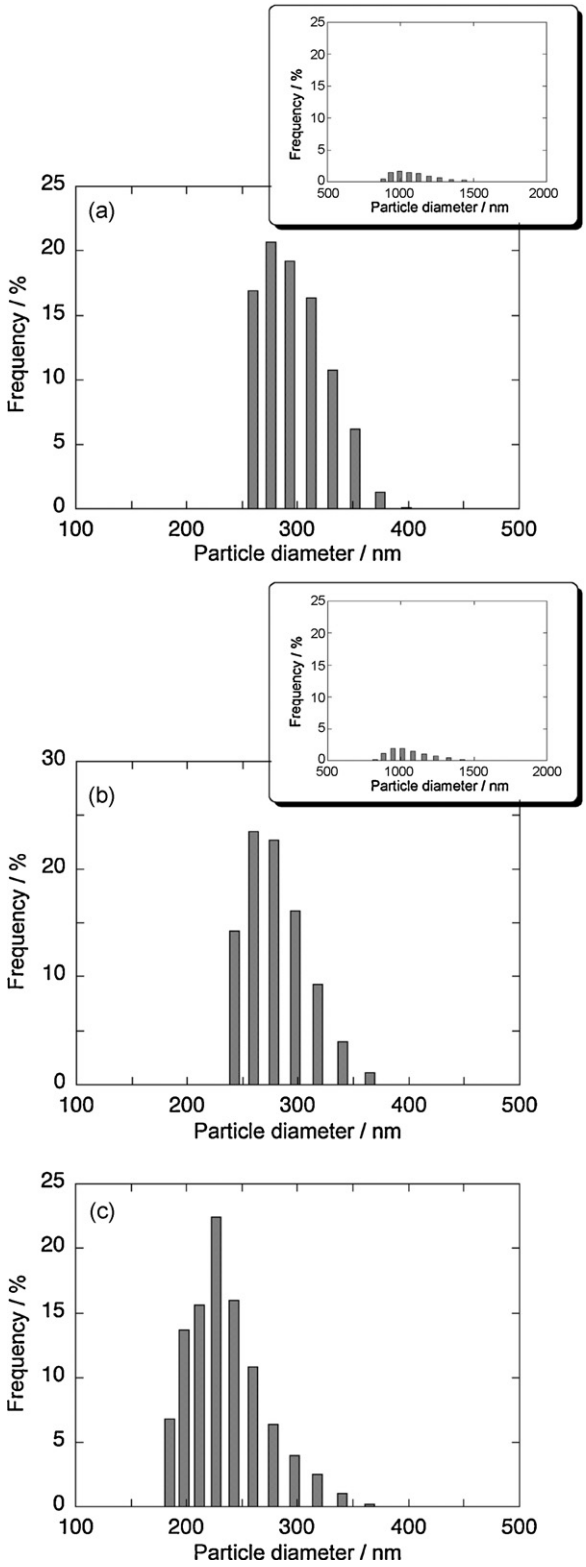

Fig. 6. Particle size distribution of PX nanoparticles ($\rho = 1.5$) obtained by DLS analyses with different PVP concentrations: (a) PX23a, (b) PX23b and (c) PX23c. The PVP concentrations of the PX23a, PX23b, and PX23c samples are 0.2, 0.3, and 0.4 mg/mL, respectively.

3.3. Formation mechanism of PX nanoparticles

By using a large lipophilic phosphazenium cation, the synthesis of anionic drug-based organic nanoparticles has been successful. It is conceivable that the PX^- and PHS^+ first contact with each other to form an ion-pair complex in aqueous solution due to a strong electrostatic attraction. The contact ion-pairs will aggregate themselves by their van der Waals interaction to produce embryos or nuclei, followed by the growth of nuclei into clusters and subsequently larger particles [28]. The produced particles are more stable at $\rho = 1.5$, indicting a positively charged particle surface [11]. A similar positively charged particle surface has been observed also for PX nanoparticles based on cationic polymer prepared by evaporation technique [3]. PVP is a representative stabilizer that is widely used in the synthesis of many metal and semiconductor nanoparticles [29] as well as a variety of other organic nanoparticles [10–12] because of its steric effects. So, this polymer would stabilize the dispersion of PX nanoparticles.

3.4. Optical properties of PX nanoparticles in aqueous solution

The spectroscopic properties of the PX nanoparticles are markedly different from those of pure PX monomer in aqueous solution. Fig. 7A shows the absorption spectra of PX nanoparticles with various mean diameters along with that of PX monomer in aqueous solution. The spectra were normalized at their peak position. It is obvious that the absorption spectra of the aqueous dispersed nanoparticles are close to that of pure PX, but have a weak shoulder at around 430 nm. This is probably caused by the ion-pair interaction between PX and PHS and by the scattering from dispersions.

The effect of particle formation on the emission spectra is significantly pronounced. Fig. 7B shows fluorescence emission spectra of pure PX and PX nanoparticles in aqueous solution, upon excitation at 350 nm. The fluorescence properties (peak position and fluorescence quantum yield Φ_f) are also summarized in Table 1. In the case of nanoparticle samples of PX23a, PX23b and PX23c with the mean diameters of 364, 368, and 232 nm, respectively, the emission intensity increased and shifted to longer wavelength from 480 to 502 nm. As can be seen in Table 1, the fluorescence quantum yields of these samples are $(0.08–0.10) \times 10^{-2}$. These values are larger than that obtained for PX monomer ($\Phi_f = 0.01 \times 10^{-2}$) in aqueous media [25]. The results demonstrate an inhibition of some efficient nonradiative channels of the PX chromophore. As mentioned earlier, PX exhibits an internal twisting motion to generate the keto rotamers in 2–5 ps [24]. Therefore, the emission enhancement with a bathochromic effect is likely attributed to the effect of intramolecular planarization induced by restriction of the twisting motion relaxation process in the solid-state PX nanoparticles. The decrease in the nonradiative pathways may lead to a decrease in phototoxicity of the PX nanoparticles as in the case of the caged drug within cyclodextrin nanocavities [30,31].

It should be noted that, for PX11a, the fluorescence intensity slightly increased but still had a low ($\Phi_f = 0.04 \times 10^{-2}$) value. In addition, the fluorescence peak wavelength was almost unchanged as compared to that of PX monomer. This indicates that the interaction is not strong enough to significantly alter their optical properties, probably making the nanoparticles less stable.

The emission characteristics of the nanoparticles of PX23a, PX23b and PX23c are close to those observed for PX within the hydrophobic pockets of human serum albumin (HSA) [20]. Hence, the observed emission of the present PX nanoparticles comes from a hydrophobic state (hydrophobic solid-state matrix of PHS), leading to a restriction of the twisted conformation and therefore reducing the nonradiative process [12]. Both intramolecular planarization and reducing the nonradiative processes would involve emission enhancement and bathochromic emission maximum. So the change in the fluorescence properties of the nanoparticles should indicate the different amount of hydrophobicity formed in the various experimental conditions.

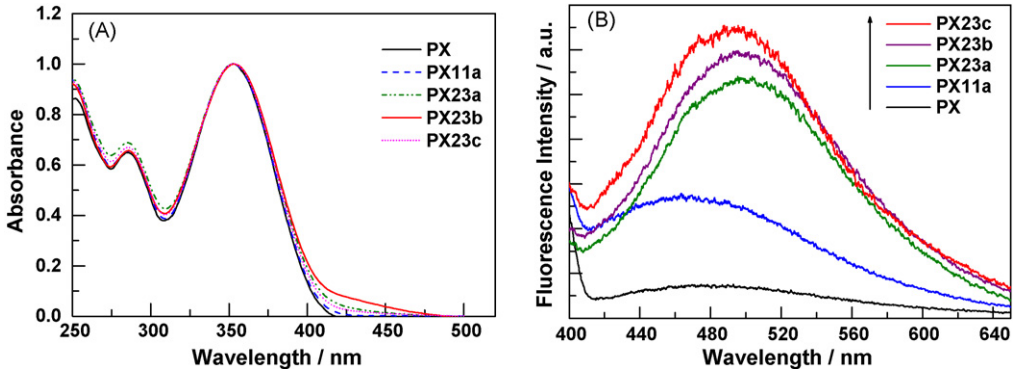

Fig. 7. (A) Absorption and (B) fluorescence spectra of pure PX and PX nanoparticles in aqueous solution prepared at different ρ values and PVP concentrations.

We finally note that PX23c nanoparticles with a relatively smaller size distribution (average diameter of 232 nm) exhibited high fluorescence quantum yield of $\Phi_f = 0.10 \times 10^{-2}$, while relatively larger nanoparticles PX23a (average diameter of 364 nm) had $\Phi_f = 0.08 \times 10^{-2}$ (Table 1). The results suggest that the optical emission properties of the PX nanoparticles are dependent on their size, which we control by modelling the molar ratio of PX with PHS and by changing the concentration of PVP. As reported by Asahi et al., the conformational structures of organic molecules confined in a small space are the key issue to explain the size dependence of nanoparticle fluorescence [32]. This size effect "Structural Confinement", is contrast to electron confinement for metals and inorganic semiconductors [32].

4. Conclusion

We have succeeded in the synthesis of anion-based piroxicam (PX) nanoparticles in pure aqueous solution without using toxic or flammable solvents. Ion association between PX drug anions and lipophilic tetrakis[tris(dimethylamino)phosphoranylidene]amino] phosphonium cations (PHS), in the presence of polyvinylpyrrolidone (PVP), produced the drug nanoparticles of 200–400 nm in water. The formation of PX nanoparticles resulted in a red-shifted fluorescence peak of about 22 nm in wavelength with an increase in the fluorescence intensity (about 10-fold enhancement) in comparison with that of the drug monomer. This is due to the involvement of the PX chromophore in the hydrophobic solid-state matrices, indicating a confinement effect of the molecule on the photophysical behaviour of the drug. We believe that this option is a valuable tool in the manufacture of new organic nanoparticles for pharmaceutical use.

Acknowledgments

We thank Prof. Keisaku Kimura (University of Hyogo) for his kind support and interest. We also thank Mrs. Masanori Saeki and Noriyuki Kitaoka (University of Hyogo) for the XRD, STEM and IR absorption measurements. The present work was supported by the JSPS Invitation Fellowship Programs for Research in Japan (S-09037) and by Grant-in-Aids for Scientific Research (B: 19310076 (H.Y.) from JSPS.

References

[1] E. Schröck, S. du Manoir, T. Veldman, B. Schoell, J. Wienberg, M.A. Ferguson-Smith, Y. Ning, D.H. Ledbetter, I. Bar-Am, D. Soenksen, Y. Garini, T. Ried, Science 273 (1996) 494–497.
[2] E.M. Merisko-Liversidge, G.G. Liversidge, Toxicol. Pathol. 36 (2008) 43–48.
[3] K. Adibkia, M.R.S. Shadbad, A. Nokhodchi, A. Javadzedeh, M. Barzegar-Jalali, J. Barar, G. Mohammadi, Y. Omidi, J. Drug Target. 15 (2007) 407–416.
[4] S.-W. Song, K. Hidajat, S. Kawi, Langmuir 21 (2005) 9568–9575.
[5] N. Sanvicens, M.P. Macro, Tends Biotechnol. 26 (2008) 425–433.
[6] L.M. Ying, A. Bruckbauer, A.M. Rothery, Y.E. Korchev, D. Klenerman, Anal. Chem. 74 (2002) 1380–1385.
[7] S. Santra, M.S. Dutta, G.A. Walter, B.M. Moudgil, Res. Treat. 4 (2005) 593–602.
[8] M.J. Rosemary, V. Suryanarayanan, P. Ganapatireddy, I. Maclaren, S. Baskaran, T. Pradeep, Proc. Indian Acad. Sci. (Chem. Sci.) 115 (2003) 703–709.
[9] (a) H. Yao, Z. Ou, K. Kimura, Chem. Lett. 34 (2005) 1108–1109;
(b) Z. Ou, H. Yao, K. Kimura, Chem. Lett. 35 (2006) 782–783.
[10] Z. Ou, H. Yao, K. Kimura, J. Photochem. Photobiol. A 189 (2007) 7–14.
[11] Z. Ou, H. Yao, K. Kimura, Bull. Chem. Soc. Jpn. 80 (2007) 295–302.
[12] H. Yao, M. Yamashita, K. Kimura, Langmuir 25 (2009) 1131–1137.
[13] E.A. Silinsh, in: M. Cardona, P. Fulde, H.J. Queisser (Eds.), Organic Molecular Crystals: Their Electronic States, Springer-Verlag, Berlin, 1980 (Chapter 1).
[14] T. Uemura, S. Kitagawa, J. Am. Chem. Soc. 125 (2003) 7814–7815.
[15] D. Xiao, L. Xi, W. Yang, H. Fu, Z. Shuai, Y. Fang, J. Yao, J. Am. Chem. Soc. 125 (2003) 6740–6745.
[16] X. Gong, T. Milic, C. Xu, J.D. Batteas, C.M. Drain, J. Am. Chem. Soc. 124 (2002) 14290–14291.
[17] K.P. Krause, O. Kayser, K. Mäder, R. Gust, R.H. Müller, Int. J. Pharm. 196 (2000) 169–172.
[18] P.C. Damiani, M. Bearzotti, M. Cabezón, A.C. Olivieri, J. Pharm. Biomed. Anal. 17 (1998) 233–236.
[19] Y.H. Kim, D.W. Cho, S.G. Kang, M. Yoon, D. Kim, J. Lumin. 59 (1994) 209–217.
[20] M. El-Kemary, M. Gil, A. Douhal, J. Med. Chem. 50 (2007) 2896–2902.
[21] D.W. Cho, Y.H. Kim, M. Yoon, S.C. Jeoung, D. Kim, Chem. Phys. Lett. 226 (1994) 275–280.
[22] R. Banerjee, H. Chakraborty, M. Sarkar, Biopolymers 75 (2004) 355–365.
[23] S. Rozou, A. Voulgari, E. Antoniadou-Vyza, Eur. J. Pharm. Sci. 21 (2004) 661–669.
[24] M. Gil, A. Douhal, Chem. Phys. 350 (2008) 179–185.
[25] S.M. Andrade, S.M.B. Costa, Phys. Chem. Chem. Phys. 1 (1999) 4213–4218.
[26] M. Henrich, A. Marhold, A.A. Kolomeitsev, N. Kalinovich, G.-V. Röschenthaler, Tetrahedron Lett. 44 (2003) 5795–5798.
[27] R. Pignatello, C. Bucolo, G. Spedalieri, A. Maltese, G. Puglisi, Biomaterials 23 (2002) 3247–3255.
[28] (a) D. Horn, J. Rieger, Angew. Chem. Int. Ed. 40 (2001) 4330–4361;
(b) B.K. An, S.K. Kwon, S.Y. Park, Angew. Chem. Int. Ed. 46 (2007) 1978–1982.
[29] (a) R. Si, Y. Zhang, L. You, C. Yan, J. Phys. Chem. B 110 (2006) 5994–6000;
(b) K. Vinodgopal, Y. He, M. Ashokkumar, F. Grieser, J. Phys. Chem. B 110 (2006) 3849–3852;
(c) E. Bekyarova, A. Hashimoto, M. Yudasaka, Y. Hattori, K. Murata, H. Kanoh, D. Kasuya, S. Iijima, K. Kaneko, J. Phys. Chem. B 109 (2005) 3711–3714;
(d) J.I. Paredes, F. Suarez-Garcia, S. Villar-Rodil, A. Martinez-Alonso, J.M.D. Tascon, J. Phys. Chem. B 107 (2003) 8905–8909;
(e) G.W. Busser, J.G. van Ommen, J.A. Lercher, J. Phys. Chem. B 103 (1999) 1651–1659;
(f) L.I. Gabaston, R.A. Jackson, S.P. Armes, Macromolecules 31 (1998) 2883–2888.
[30] M. El-Kemary, A. Douhal, in: A. Douhal (Ed.), Cyclodextrin Materials Photochemistry, Photophysics and Photobiology, Elsevier, 2006 (Chapter 4).
[31] P. Bortolus, S. Monti, Adv. Photochem. 21 (1996) 1–133.
[32] T. Asahim, T. Sugiyama, H. Masuhara, Acc. Chem. Res. 41 (2008) 1790–1798.